

Single-Atom Catalysis

How to cite:

International Edition: doi.org/10.1002/anie.202207524

German Edition: doi.org/10.1002/ange.202207524

Selectively Coupling Ru Single Atoms to PtNi Concavities for High-Performance Methanol Oxidation via *d*-Band Center Regulation

Fanpeng Kong, Xiaozhi Liu, Yajie Song, Zhengyi Qian, Junjie Li, Lei Zhang, Geping Yin, Jiajun Wang,* Dong Su,* and Xueliang Sun*

Abstract: Single atom tailored metal nanoparticles represent a new type of catalysts. Herein, we demonstrate a single atom-cavity coupling strategy to regulate performance of single atom tailored nano-catalysts. Selective atomic layer deposition (ALD) was conducted to deposit Ru single atoms on the surface concavities of PtNi nanoparticles (Ru-ca-PtNi). Ru-ca-PtNi exhibits a record-high activity for methanol oxidation reaction (MOR) with $2.01 \text{ A mg}^{-1}_{\text{Pt}}$. Also, Ru-ca-PtNi showcases a significant durability with only 16% activity loss. Operando electrochemical Fourier transform infrared spectroscopy (FTIR) and theoretical calculations demonstrate Ru single atoms coupled to cavities accelerate the CO removal by regulating *d*-band center position. Further, the high diffusion barrier of Ru single atoms in concavities accounts for excellent stability. The developed Ru-ca-PtNi via single atom-cavity coupling opens an encouraging pathway to design highly efficient single atom-based (electro)catalysts.

Introduction

The electro-oxidation of methyl alcohol plays an important role in the low-temperature fuel cells, bio-mass conversion and fine chemistry.^[1] Pt–M binary alloy has displayed their excellent activity towards methanol oxidation reaction (MOR) by regulating coordinative environment of Pt.^[2] However, the main intermediate, CO, drastically poisons the

catalytic center owing to their strong affinity.^[3] Although alloying Pt with oxophilic metal, such as Ru, can mitigate the CO poisoning issues to a certain extent, Pt–Ru alloy still suffers from the limited synergistically active center owing to their random distribution.^[4] For instance, PtRu alloy featuring a Pt-rich core and a Ru-rich shell, was demonstrated by the Chen's group through X-ray absorption spectra,^[5] in line with the Danberry's observation via the ¹⁹⁵Pt electrochemical nuclear magnetic resonance.^[6]

Single-atom tailoring strategy is capable to maximize the active center due to its highly uniform dispersion.^[7] Besides, the unique electronic structure and unsaturated coordinative environment has been demonstrated to benefit the CO removal.^[8] Karim et al. showcased that Ir single atoms tailored MgAl₂O₄ exhibited the high activity for low-temperature CO oxidation.^[9] Ru single atoms modulating CeO₂ accelerated the CO removal as compared to CeO₂.^[10] Considering Ru single atom is an efficient promoter for CO oxidation, using Ru single atom to tailor Pt based catalysts is expected to enhance the methanol oxidation by mitigating CO poisoning. However, the different intrinsic segregation energy of Ru in comparison of Pt as well as the high surface energy of single atoms lead to the poor durability of achieved catalysts.^[2,11] Up to now, single atom tailoring metal catalysts have been reported by many groups, but stabilization of them is rarely explored. Spatial confinement is one of the strategies for the stabilization of single atom.^[12] Several works have utilized the spatial isolation strategy to fabricate the various metal single atoms supported on carbon matrix.^[13] For example, Li et al. observed that Ir single sites were anchored into the nitrogen-doped carbon through spatial isolation.^[14] Single Pt atoms were successfully confined into metal-organic framework by Jiang's group.^[15] Unfortunately, the similar property of metal surface poses a huge challenge towards selectively entrapping single atoms into the designated confinement sites. Understanding single-atom position control chemistry is of significance for stabilizing single atom tailoring metal catalysts. Additionally, the effect of coupling between single atoms and confined space on electro-catalytical activity is still unclear and rarely explored.

Herein, we synthesized hybrid catalysts of Ru single atoms coupled to the surface cavities of PtNi NPs (Ru-ca-PtNi) via selective ALD technique where the Ru single atoms were exclusively trapped into the concave domain. This catalyst shows an improved peak mass activity for MOR, $2.01 \text{ A mg}^{-1}_{\text{Pt}}$, which is a 5.8-fold enhancement in comparison with the commercial Pt/C. Transmission elec-

[*] F. Kong, Y. Song, Z. Qian, G. Yin, J. Wang
 MIIT Key Laboratory of Critical Materials Technology for New Energy Conversion and Storage, Harbin Institute of Technology Harbin (China)
 E-mail: jjjunhit@hit.edu.cn

F. Kong, J. Li, L. Zhang, X. Sun
 Department of Mechanical and Materials Engineering, University of Western Ontario
 London (Canada)
 E-mail: xsun9@uwo.ca

X. Liu, D. Su
 Institute of Physics, Chinese Academy of Sciences
 Beijing (China)
 E-mail: dongsu@iphy.ac.cn

J. Wang
 Chongqing Research Institute, Harbin Institute of Technology
 Chongqing (China)

tron microscopy results suggest that Ru single atoms are anchored in the concave domains in Ru-ca-PtNi, as compared to the reference catalysts where Ru single atoms are located on the smooth surface of PtNi NPs (Ru-su-PtNi). According to operando FTIR analysis and density functional theory (DFT) calculations, the Ru single atom-cavity synergistic coupling efficiently accelerates the CO removal by optimizing the *d*-band center position. Further, our theoretical analysis indicates a high diffusion barrier for the Ru atoms trapped by cavities, thus, accounting for the remarkably enhanced stability of Ru-ca-PtNi. This work demonstrates a single atom-cavity coupling mechanism to enhance the activity and stability of single atom-based catalysts.

Results and Discussion

Ru single atoms were deposited into the concavity of PtNi substrate with corrugated surface, denoted as Ru-ca-PtNi via surface decoration and followed selective ALD (Figure 1). Firstly, highly dispersed PtNi NPs on carbon support was prepared by a wet-chemistry synthetic method (Figure S1). The PtNi NPs were then dispersed into the ethanol solution containing oleylamine, where metal substrate surface was decorated with spontaneously adsorbed oleylamine molecule with the boiling point of 364.4 °C (Figure S2). The oleylamine decorated PtNi NPs were further immersed into acid solution to corrugate the surface (denoted as ca-PtNi), as shown in Figure S3. There was no oleylamine decoration on the new formed concavity owing to the dissolution of Ni atoms. The Ru atoms can be only deposited into the cavities during ALD because adsorbed oleylamine and carbon impeded the deposition of Ru, demonstrated by our previous work.^[16] The element quantification derived from XPS analysis also demonstrates the absence of Ru for oleylamine decorated PtNi NPs without acid wash (Fig-

ure S4). Thus, it is rationally speculated that Ru atoms can exclusively deposit into the newly formed concave areas of Ru-ca-PtNi. In the final step, clean Ru-ca-PtNi was obtained by removing adsorbed oleylamine in acetic acid where the surface cleanliness was demonstrated by the observation of H_{UPD} region in the cyclic voltammetry curves (Figure S5). To verify if Ru single atoms were located in the surface caves in Ru-ca-PtNi, a reference sample with Ru single atom deposited on the smooth surface of PtNi was made through ALD strategy (denoted as Ru-su-PtNi), where the smoothing of metal substrate was achieved by thermal-driven segregation (Figure S6). It is noted that Ru-ca-PtNi exhibits a lower value of relative Ru content as compared to Ru-su-PtNi, likely arising from the suppression of Ru atoms deposition by oleylamine (Figure S4).

The electro-catalytical performance of Ru-ca-PtNi towards MOR is evaluated in three-electrode system as shown in Figure 2. The observation of typical H atom adsorption/desorption and the oxidation/reduction of Pt regions demonstrates majority of Pt atoms at surface (Figure 2a). MOR test results demonstrate the highest electro-catalytical activity on Ru-ca-PtNi based on the onset potential and peak current density (Figure 2b). The similar activity between Pt and PtNi may be attributed to their similar electronic structure. For Ru-ca-PtNi, the lower work potential and Tafel slop value are required to achieve the current density of 5 mA cm^{-2} during MOR, thus, demonstrating its superior activity (Figure 2c). Further, the turnover of frequency (TOFs) derived from XPS and ECSA analysis, quantitatively indicates the highest intrinsic activity on Ru-ca-PtNi (Figure 2d). Besides, Ru-ca-PtNi exhibits the highest MOR performance with mass activity of $2.01 \text{ A mg}^{-1}_{\text{Pt}}$ at the peak of current density, which is 5.8 times and 3.2 times as compared with that of Pt/C and Ru-su-PtNi, respectively (Figure 2e). The superior MOR activity on Ru-ca-PtNi is also demonstrated by the chronoamperometry test (Figure S7). Additionally, Ru-ca-PtNi

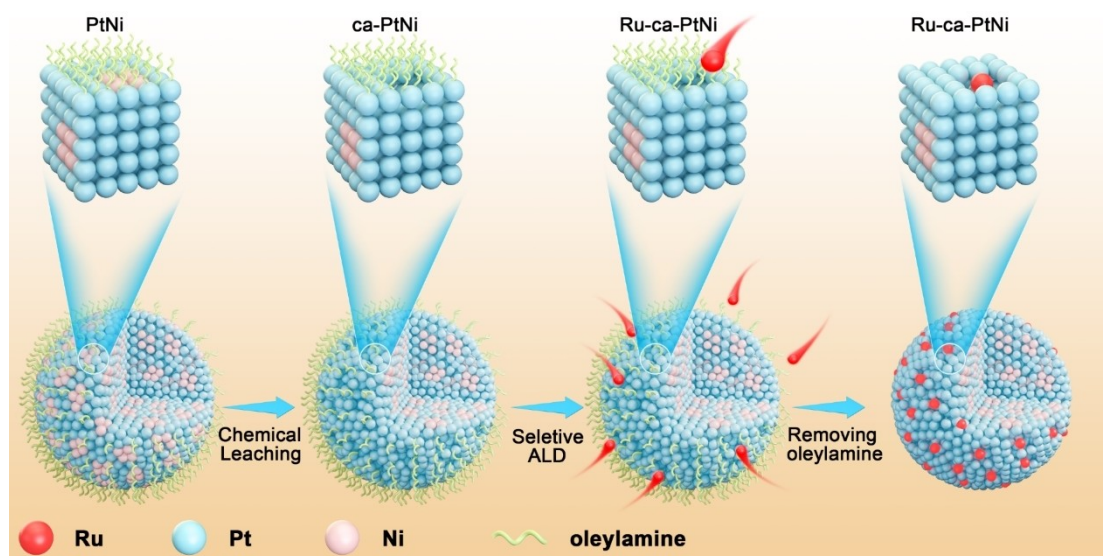


Figure 1. Schematic diagram for fabrication of Ru-ca-PtNi through selective atomic layer deposition.

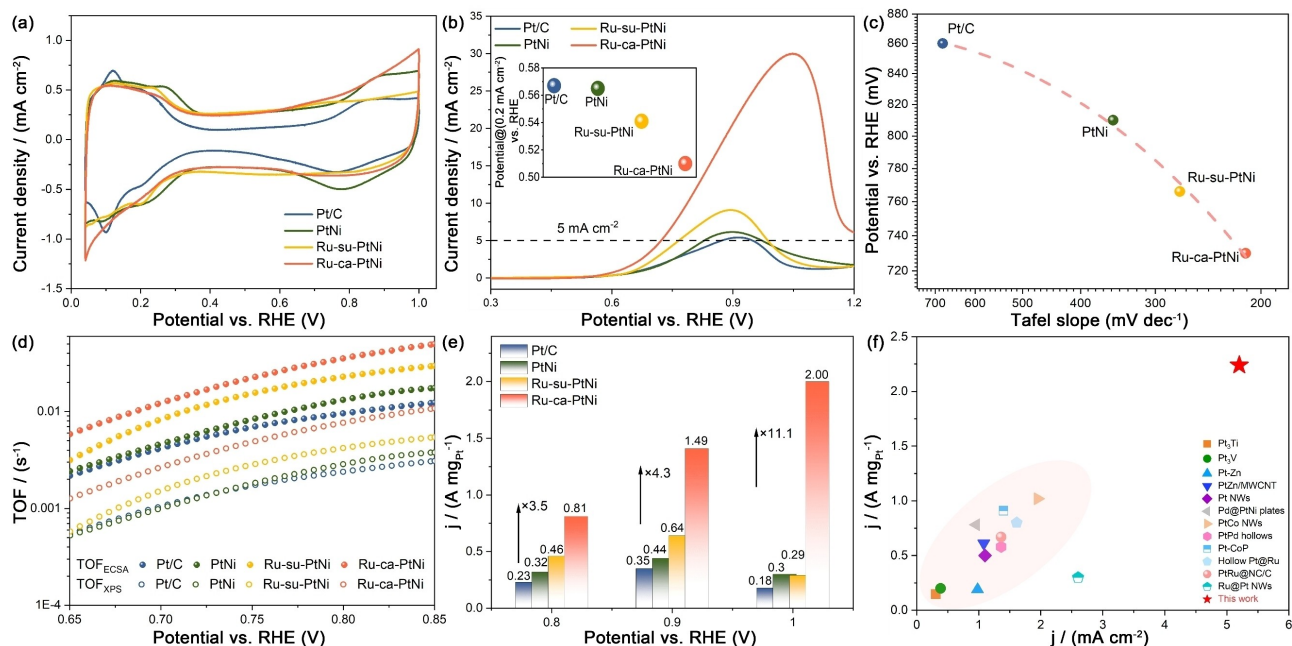


Figure 2. a) CV curves of Pt/C, PtNi, Ru-su-PtNi, and Ru-ca-PtNi in argon saturated 0.1 M HClO₄. b) CV curves of Pt/C, PtNi, Ru-su-PtNi, and Ru-ca-PtNi in argon saturated 0.5 M methanol + 0.1 M HClO₄ mixed solution. The inset dictates the potential of different catalysts when current density achieves 0.2 mA cm⁻². c) The potential and Tafel slope obtained from MOR polarization curves at the loaded Pt atoms at different densities of 0.2 mA cm⁻². d) TOFs of Pt/C, PtNi, Ru-su-PtNi, and Ru-ca-PtNi on basis of the loaded Pt atoms at different potentials. e) Mass activities of Pt/C, PtNi, Ru-su-PtNi, and Ru-ca-PtNi for MOR. f) The mass activity and specific MOR activity of Ru-ca-PtNi at peak in comparison of that of other Pt-based catalysts in literature.

also represents one of the best MOR catalysts on basis of mass activity and specific activity (Figure 2f), indicating that the single atom-cavity coupling plays an important role towards electrocatalytic kinetics of single atoms-based catalysts.

In order to understand the superior MOR activity on Ru single atom tailored Pt-rich catalysts, electrochemical operando FTIR measurements on Ru-ca-PtNi are conducted to understand MOR at the molecular-level. The negative bands at ≈ 2300 and 2050 cm^{-1} in operando FTIR tests (Figure 3a,b, Figure S8), are assigned to CO₂ and linearly bonded CO (CO_L), respectively.^[17] The observation of CO infrared peaks directly demonstrates that CO is a main product during MOR process, which subsequently strongly poisons active sites. It is noted that the ratio of CO₂ to CO infrared peak intensity in the case of Ru-ca-PtNi is critically higher than that of Pt/C (Figure 3c,d). CO and CO₂ infrared peak intensity at different potentials are quantified to understand reaction mechanism (Figure 3e). The first finding is that the CO₂ peak intensity quickly increases with the decreasing CO peak intensity, thus signifying the removal of CO for MOR. The other finding is that the presence of Ru single atoms benefits the removal of CO, thus accounting for the significantly enhanced MOR performance on Ru single atoms tailored nanocatalysts. It is noted that the Ru-ca-PtNi is more beneficial for the methanol oxidation on basis of the variation of normalized CO and CO₂ peak intensity compared to Ru-su-PtNi (Figure 3e), indicating the positive effect of single atom-cavity coupling on the CO

removal ability of Pt based catalysts. CO stripping tests are further conducted to evaluate the CO-removal ability of electrocatalysts (Figure S9).^[18] For Ru-ca-PtNi and Ru-su-PtNi, the obviously negative shift of onset potential supports that the presence of Ru atoms is beneficial for the CO oxidation. Besides, their onset potential is almost the same as that of PtRu alloy, suggesting that Ru atoms also promote the CO removal through bi-functional mechanism because of its high activity towards the water activation (Figure S9).^[19] Considering the inhomogeneous dispersion of active center in hetero-catalysts, the average CO oxidation potential is further calculated to evaluate CO stripping ability.^[20] The average CO oxidation potential of 0.72 V for Ru-ca-PtNi is noted to be lower than that of Pt/C by 100 mV, thus significantly enhancing MOR activity by accelerating the removal of CO.

Exploring the local chemical and coordinative environment of Ru-ca-PtNi benefits to understand its obviously accelerated electrocatalytic kinetics. The almost same XRD patterns of Ru-ca-PtNi and Ru-su-PtNi prove the absence of Ru and Ru oxides with long-range structure (Figure S10). XPS as a surface-sensitive characterization is conducted to study their electronic structure (Figure S11). The Ru 3p XPS in the case of Ru-ca-PtNi exhibits similar oxidation state in comparison with Ru-su-PtNi (Figure S12). For the Pt 4f XPS spectra of Ru-ca-PtNi, the shifted peak towards high binding energy as compared to c-PtNi and Pt demonstrates the tailored electronic structure by incorporated Ru atoms (Figure 4a, S13 and Table S1). The surface electronic

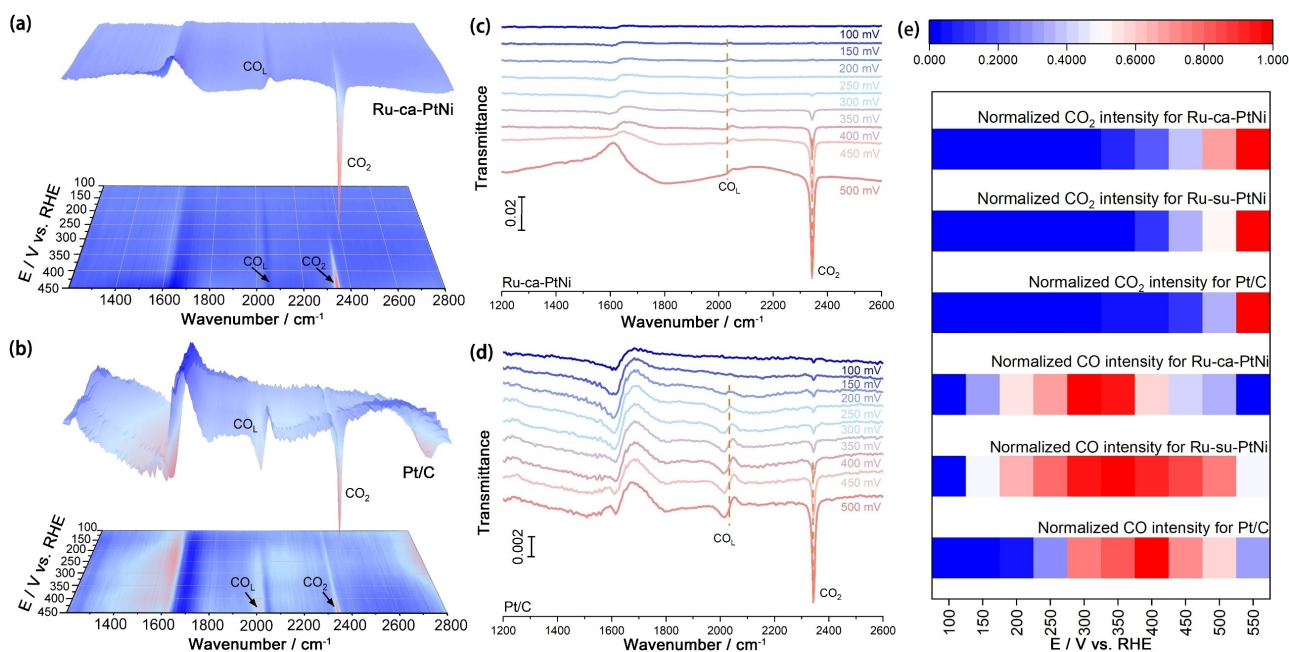


Figure 3. Three-dimensional operando FTIR spectra on a) Ru-ca-PtNi and b) Pt/C in argon saturated 0.5 M methanol + 0.1 M HClO₄ mixed solution. Operando FTIR spectra on c) Ru-ca-PtNi and d) Pt/C at different potentials in argon saturated 0.5 M methanol + 0.1 M HClO₄ mixed solution. e) The normalized CO and CO₂ intensity of Pt/C, Ru-su-PtNi and Ru-ca-PtNi at different potentials, obtained from the integral of CO and CO₂ FTIR peaks.

structure and *d*-band structure is further studied by using surface valence band spectra, which is collected on the nanoparticle monolayers by high-resolution XPS (Figure 4b).^[21] The *d*-band center of Ru-ca-PtNi is positioned at -2.98 eV, as compared to -3.03 eV for Ru-su-PtNi. The obvious upshift of *d*-band centers of Ru-ca-PtNi can be ascribed to the redistribution of surface *d*-states by the single atom-cavity coupling.^[22] In addition, the positive shift of *d*-band centers has been observed to benefit the methanol oxidation through tailoring the binding strength between catalysts and adsorbates.^[22a]

Synchrotron radiation-based X-ray absorption near edge structure (XANES) and extended X-ray absorption fine structure (EXAFS) are employed to shed light on the chemical structure of Ru-ca-PtNi. The XANES profiles demonstrate the similar cationic Ru environment for Ru-ca-PtNi and Ru-su-PtNi, where their valence state is located between metallic Ru⁰ and oxidizing Ru⁴⁺ (Figure 4c and Figure S14). For Ru-ca-PtNi, the absence of periodic oscillation excludes the presence of long-range ordered Ru local structure, evidencing their delocalized nature. The Fourier transforms (FT) k^2 -weighted $\chi(k)$ -function of Ru EXAFS is shown in Figure 4d. The atomic dispersion of Ru for Ru-ca-PtNi is demonstrated by the absence of metallic Ru–Ru and Ru–O–Ru coordination, which are corresponding to the FT peak at 2.5 Å and 3.2 Å, respectively. Wavelet transform (WT) of EXAFS oscillation is further performed to gain more insights pertaining to coordination information. The maximum in the contour line plot for Ru-ca-PtNi is observed at $k=3.0$ Å⁻¹, also demonstrating the formation of mono-dispersed Ru atoms in the cavities (Figure 4e). The observed

shift in the maximum intensity is possibly owing to the different coordination environment of Ru single atoms for Ru-ca-PtNi and Ru-su-PtNi, in line with the results of fitting spectra (Figure S15 and Table S2).

Atomically revealing Ru atoms distribution on Pt based substrate is beneficial for understanding the structure difference and further performance enhancement. Aberration-corrected high angle annular dark field-scanning transmission electron microscopy (HAADF-STEM) has been conducted to characterize the local structure of catalysts (Figure 5a and Figure S16). It is observed that the nanoparticles of Ru-ca-PtNi have a multi-grain nature and show a highly curved surface (Figure 5a), whereas the Ru-su-PtNi sample are single-grained nanoparticles with smooth surface (Figure 5c). Enlarged HAADF image of a representative Ru-ca-PtNi at the edge is shown in Figure 5d while that of the Ru-su-PtNi sample is shown in Figure 5f. These results show the Ru-ca-PtNi sample indeed has a corrugated surface. Although the distribution of Ru can not be directly distinguished from the contrast of atomic resolution HAADF images. Its existence can be verified from Figure 5b and Figure S17 where the electron energy loss spectroscopy (EELS) signals of Ru–L and Pt–M edges are shown. In addition, the high-resolution energy dispersive spectroscopy (EDS) mapping demonstrates atomically dispersed Ru single atom (Figure 5e). These observations are in line with the XAFS and XPS results, which indicate the corrugated surface of Ru-ca-PtNi sample can be the host sites of Ru single atoms.

Besides the STEM results, the partial density of states (PDOS) for different catalysts with CO adsorption are also

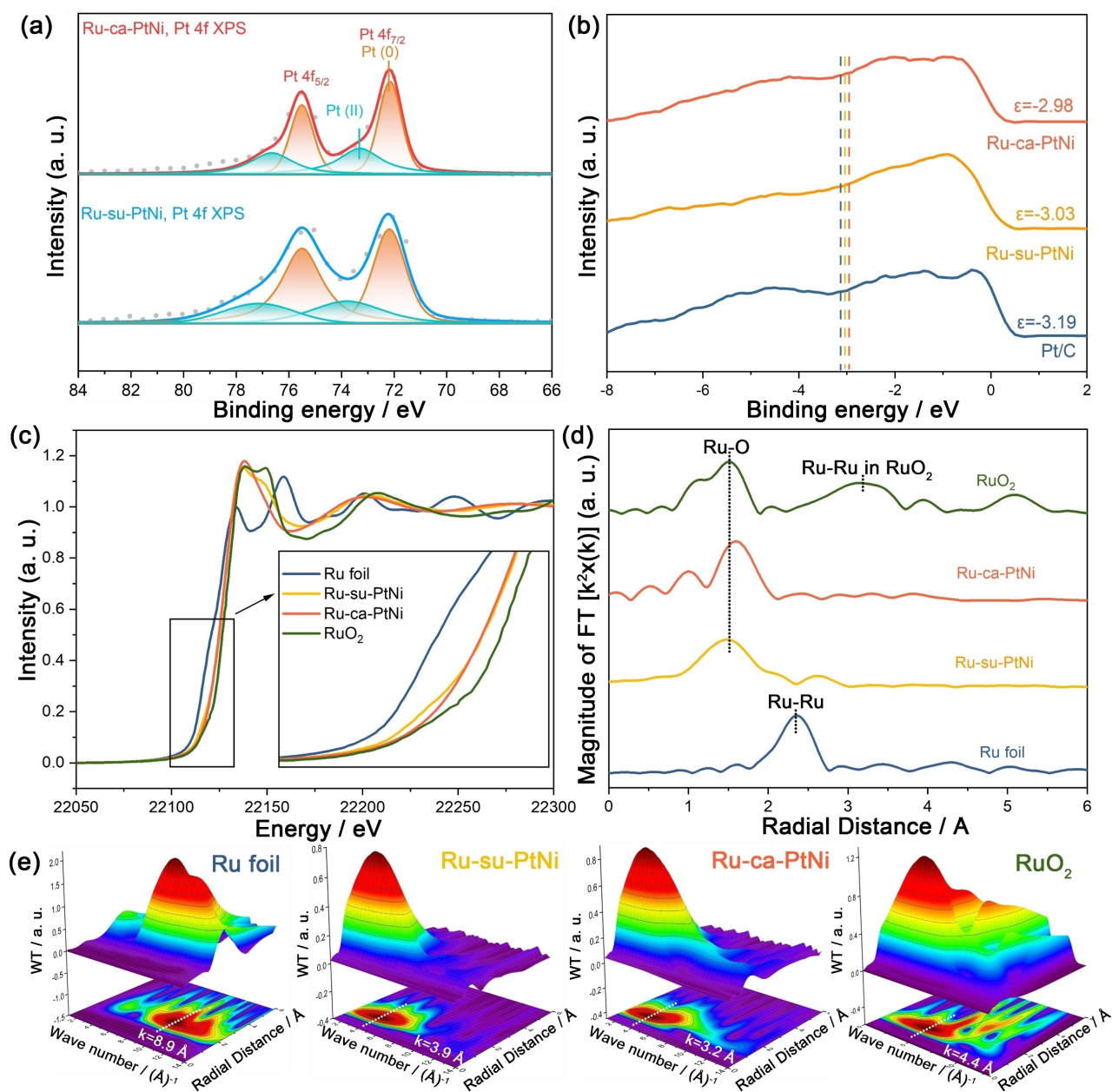


Figure 4. a) The XPS spectra of Ru-ca-PtNi and Ru-su-PtNi. b) Surface valence band photoemission spectra of Ru-ca-PtNi, Ru-su-PtNi and Pt/C. The Ru K edge XANES (c) and EXAFS (d) spectra of Ru-ca-PtNi, Ru-su-PtNi, Ru foil and RuO₂; e) Wavelet transforms for the k^2 -weighted Ru K-edge EXAFS signal of Ru-ca-PtNi, Ru-su-PtNi, Ru foil and RuO₂.

calculated to further rationalize the differences in adsorption properties of CO on Pt and Ru-ca-PtNi (Figure 5g and Figure S18). The Pt d -band centers in the case of Ru-ca-PtNi locates relatively from the Fermi level in comparison with Pt, in line with the valence band analysis. In fact, the up-shift of d -band center leads to the strong adsorption of adsorbates owing to the reduced occupancy of anti-bonding orbitals.^[23] Ru-ca-PtNi with the up-shifted d -band center exhibits the strongest binding energy with OH* formed through water activation, and further boosts the CO* removal (Figure S19 and S20).^[3c,24] The outstanding CO stripping ability of Ru single atom tailored catalysts demon-

strates the bi-functional mechanism owing to its high activity towards the water activation.^[19] And the up-shift of d -band center is the electronic origin, which strengthens the binding with OH*. Tailored electronic structure and bi-functional mechanism are proposed to account for the enhanced MOR activity. It is also speculated that the up-shift of d -band center for Ru-ca-PtNi accounts for the higher MOR in comparison with the Ru-su-PtNi, considering that their similar CO average potential (Figure S9). Besides, the reaction mechanism of methanol oxidation is further investigated by density functional theory (DFT) calculations ($U = 0.8$ V vs. RHE, Figure 5h).^[8a,24a] Ru-ca-PtNi exhibits more

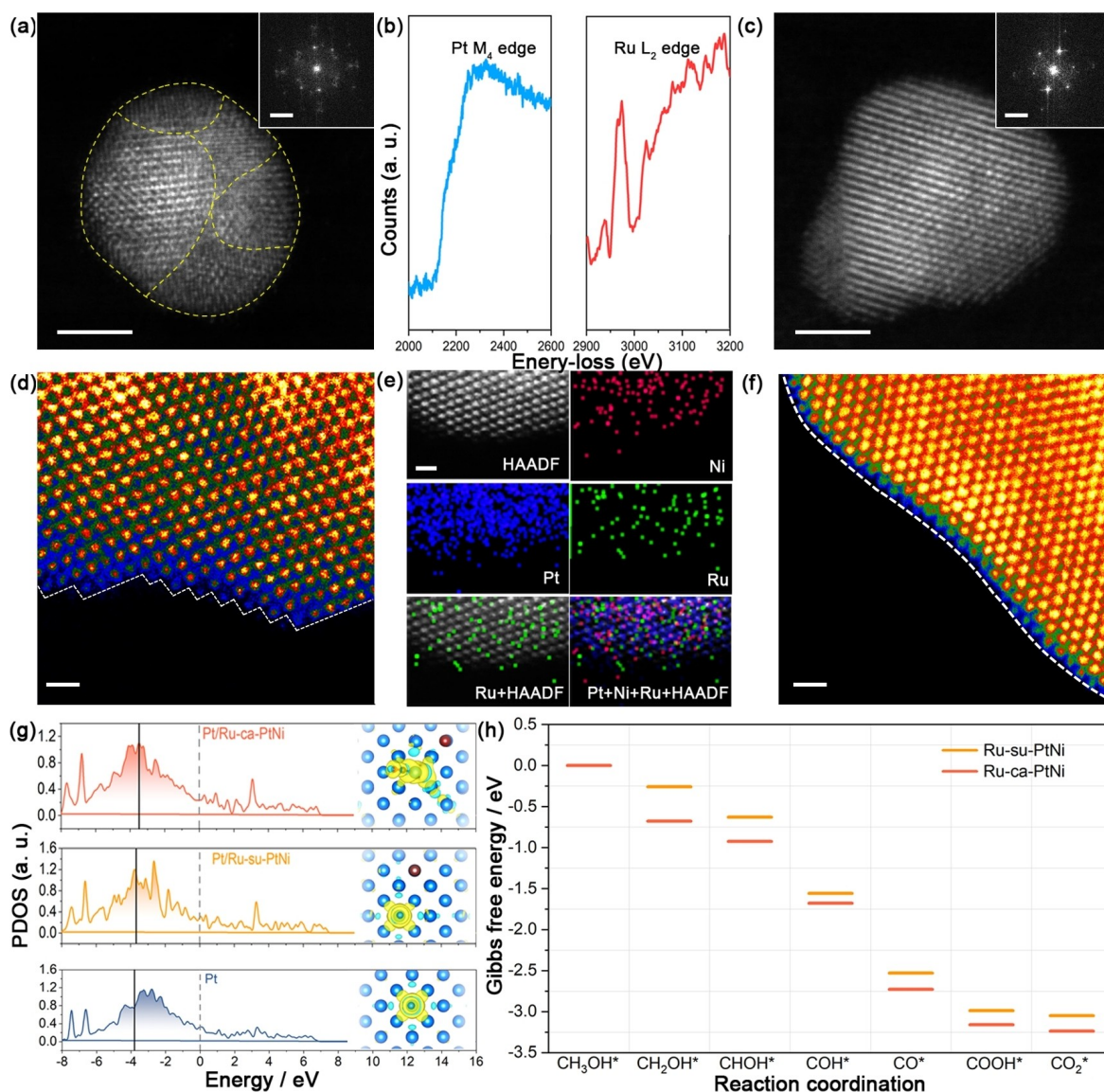


Figure 5. a) The aberration-corrected HAADF-STEM image of Ru-ca-PtNi (the scale bar is 2 nm). The inset is the corresponding FFT pattern (the scale bar is 5 nm^{-1}). b) The EELS spectra of Pt M_4 edge and Ru L_2 edge obtained from Ru-ca-PtNi. c) The HAADF-STEM image of Ru-su-PtNi (the scale bar is 2 nm). The inset is the corresponding FFT pattern (the scale bar is 5 nm^{-1}). d) The HAADF-STEM image of Ru-ca-PtNi with pseudocolor (the scale bar is 0.5 nm). e) The HAADF-STEM image of Ru-ca-PtNi and its EDS mapping (the scale bar is 0.5 nm). f) The HAADF-STEM image of Ru-su-PtNi with pseudocolor (the scale bar is 0.5 nm). g) PDOS of surface Pt atom with pre-adsorbed CO for Pt, Ru-su-PtNi and Ru-ca-PtNi. Ru atom, brown ball; Ni atom, green ball; Pt atom, light blue; C atom, black; O atom, red. h) Reaction profile for MOR on different surfaces.

energetically favorable pathway and lower overpotential in comparison with Ru-su-PtNi (Figure S21). In addition, all elementary steps are exothermic, demonstrating the superior MOR activity on Ru-ca-PtNi through single atom-cavity coupling.

The segregation of single atom during reaction inevitably deteriorates the structure of catalytic center, thus, obviously lowering reaction dynamics.^[13a] The corresponding polarization curves after stability tests consisting 3000 potential cycles between 0 V and 1.2 V in argon saturated 0.5 M methanol and 0.1 M HClO_4 mixed solution, are shown in Figure S22. It is worth noting that Ru-ca-PtNi exhibits the

considerably enhanced stability with only 16 % performance loss after stability test in comparison with ≈ 50 % performance loss for Ru-su-PtNi (Figure 6a). The obvious stability difference between Ru-ca-PtNi and Ru-su-PtNi can be reasonably attributed to single atom-cavity coupling interaction. The CO stripping with highly surface-sensitive nature is firstly tested to gain insight into the evolution of surface structure (Figure S23). The only 20-mV positive shift in average CO oxidation potential is observed in the case of Ru-ca-PtNi, in contrast with the observed 70-mV positive shift for Ru-su-PtNi (Figure 6b). For Ru-ca-PtNi and Ru-su-PtNi, the obvious difference in the variation of average CO

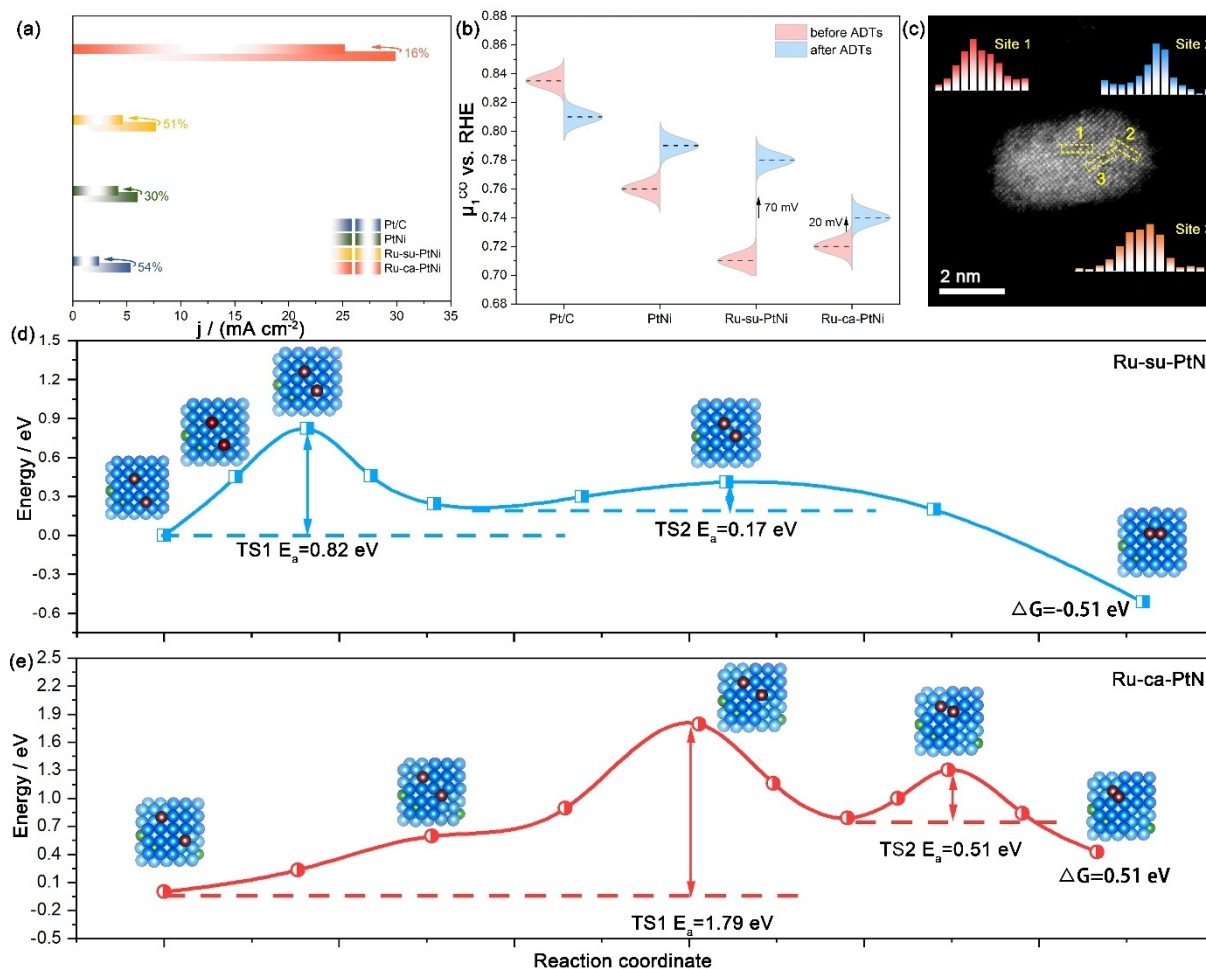


Figure 6. a) The performance loss of different catalysts after stability test. b) The average CO oxidation potential change of different catalysts after stability test. c) The HAADF-STEM image of representative aged Ru-ca-PtNi NP and corresponding intensity profile. Calculated energies along the sintering pathway of the Ru atom from Ru single atom to Ru₂ cluster by CI-NEB for Ru-su-PtNi (d) and Ru-ca-PtNi (e). Ru atom, brown ball; Ni atom, green ball; Pt atom at surface, blue ball; Pt atom at second surface, light blue.

oxidation potential is likely associated with the difference of local environment of active center. The aberration-corrected HAADF-STEM is further employed to explore their local environment. The HAADF-STEM coupled with EELS spectrum evidences the confined Ru single atom by cavities in the case of Ru-ca-PtNi (Figure 6c and Figure S24), in contrast with the observation of Ru clusters for Ru-su-PtNi (Figure S25). The absence of Ru clusters for Ru-ca-PtNi demonstrates the strong confinement of Ru atom in cavities. Climbing image nudged-elastic-band (CI-NEB) method is conducted to demonstrate the confinement of single atom by cavities. Transition states of Ru atoms sintering are then searched through CI-NEB method (Figure 6d, 6e and Figure S26). The formation of a Ru₂ cluster on Ru-ca-PtNi from the aggregation of Ru atoms requires a barrier of 1.79 eV to be overcome, as well as an endothermy of 0.51 eV. However, the diffusion barrier for such a sintering process is only 0.82 eV with an exothermicity of 0.51 eV in the case of Ru-su-PtNi. Therefore, the atomical Ru atoms are dominated in the concavity of corrugated surface during stability test in compared to the case with absence of cavities

owing to the higher kinetic diffusion barrier under the presence of cavities.

Conclusion

This work unveils the effect of single atom-cavity coupling on the activity and stability of Ru single atom tailored PtNi NPs. The atomically dispersed Ru atom anchored into the cavity, synthesized by selective ALD, is observed through the aberration-corrected HAADF-STEM images and XAFS. Also, the extraordinary electrocatalytic MOR activity is observed on Ru-ca-PtNi, which outperforms most of published results. DFT calculation and operando electrochemical FTIR analysis confirms that immobilized Ru atoms into concavities efficiently accelerate the removal of CO during MOR process by regulating the *d*-band center. In addition, the only 20% loss in performance after stability test is observed on Ru-ca-PtNi, in comparison with nearly 50% loss for Ru-su-PtNi. Structural characterization confirms the atomic dispersion of confined Ru atom in cavities

without segregation for Ru-su-PtNi. Further, the DFT simulation indicates that the higher diffusion barrier is needed to be overcome for Ru-ca-PtNi, beneficial for their structural stability. The development of Ru-ca-PtNi catalysts by single atom-cavity coupling represents a highly efficient approach to design the advanced single atom tailored metal NPs catalysts with excellent activity and stability.

Experimental Section

Essential Experimental Procedures are provided in the Supporting Information.

Acknowledgements

F. P. Kong and L. Zhang thanks the support from National Natural Science Foundation of China (Grant No. 22102041, 22075203); F. P. Kong thanks the support from China Postdoctoral Science Foundation (Grant No. 2020TQ0084); J. Wang thanks the support from “the Fundamental Research Funds for the Central Universities” (Grant No. HIT.OCEF.2021028); This work was also supported by the Natural Sciences and Engineering Research Council of Canada (NSERC), Canada Research Chair Program (CRC), Canada Foundation for Innovation (CFI), and University of Western Ontario. D. Su acknowledges the support of Strategic Priority Research Program (B) (No. XDB33030200) of Chinese Academy of Sciences; XAS measurements were conducted at hard X-ray microanalysis (HXMA) beamline at the Canadian Light Source (CLS); Electron microscopy research was performed at Chinese Academy of Sciences (X. Liu and D. Su).

Conflict of Interest

The authors declare no conflict of interest.

Data Availability Statement

The data that support the findings of this study are available from the corresponding author upon reasonable request.

Keywords: Concavity · Corrugation · Methanol Oxidation · Operando FTIR · Single Atom

- [1] a) A. Badalyan, S. S. Stahl, *Nature* **2016**, *535*, 406–410; b) L. Huang, X. Zhang, Q. Wang, Y. Han, Y. Fang, S. Dong, *J. Am. Chem. Soc.* **2018**, *140*, 1142–1147; c) A. A. Dubale, Y. Zheng, H. Wang, R. Huebner, Y. Li, J. Yang, J. Zhang, N. K. Sethi, L. He, Z. Zheng, W. Liu, *Angew. Chem. Int. Ed.* **2020**, *59*, 13891–13899; *Angew. Chem.* **2020**, *132*, 13995–14003; d) T. He, W. Wang, F. Shi, X. Yang, X. Li, J. Wu, Y. Yin, M. Jin, *Nature* **2021**, *598*, 76–81; e) N. Tian, B.-A. Lu, X.-D. Yang, R. Huang, Y.-X. Jiang, Z.-Y. Zhou, S.-G. Sun, *Electrochem. Energy Rev.* **2018**, *1*, 54–83.

- [2] J. Mao, W. Chen, D. He, J. Wan, J. Pei, J. Dong, Y. Wang, P. An, Z. Jin, W. Xing, H. Tang, Z. Zhuang, X. Liang, Y. Huang, G. Zhou, L. Wang, D. Wang, Y. Li, *Sci. Adv.* **2017**, *3*, e1603068.
- [3] a) H.-S. Chen, T. M. Benedetti, J. Lian, S. Cheong, P. B. O'Mara, K. O. Sulaiman, C. H. W. Kelly, R. W. J. Scott, J. J. Gooding, R. D. Tilley, *ACS Catal.* **2021**, *11*, 2235–2243; b) W. Liang, Y. Wang, L. Zhao, W. Guo, D. Li, W. Qin, H. Wu, Y. Sun, L. Jiang, *Adv. Mater.* **2021**, *33*, 2100713; c) Y. Wang, M. Zheng, Y. Li, C. Ye, J. Chen, J. Ye, Q. Zhang, J. Li, Z. Zhou, X.-Z. Fu, J. Wang, S.-G. Sun, D. Wang, *Angew. Chem. Int. Ed.* **2022**, *61*, e2100713; *Angew. Chem.* **2022**, *134*, e2100713; d) A. Shan, S. Huang, H. Zhao, W. Jiang, X. Teng, Y. Huang, C. Chen, R. Wang, W.-M. Lau, *Nano Res.* **2020**, *13*, 3088–3097.
- [4] a) L. Xiong, Z. Sun, X. Zhang, L. Zhao, P. Huang, X. Chen, H. Jin, H. Sun, Y. Lian, Z. Deng, M. H. Rummerli, W. Yin, D. Zhang, S. Wang, Y. Peng, *Nat. Commun.* **2019**, *10*, 3782; b) D.-J. Chen, Y. J. Tong, *Angew. Chem. Int. Ed.* **2015**, *54*, 9394–9398; *Angew. Chem.* **2015**, *127*, 9526–9530; c) Z. Zhang, Z. Luo, B. Chen, C. Wei, L. Zhao, J. Chen, X. Zhang, Z. Lai, Z. Fan, C. Tan, M. Zhao, Q. Lu, B. Li, Y. Zong, C. Yan, G. Wang, Z. J. Xu, H. Zhang, *Adv. Mater.* **2016**, *28*, 8712–8717; d) W. Huang, H. Wang, J. Zhou, J. Wang, P. N. Duchesne, D. Muir, P. Zhang, N. Han, F. Zhao, M. Zeng, J. Zhong, C. Jin, Y. Li, S.-T. Lee, H. Dai, *Nat. Commun.* **2015**, *6*, 10035; e) R. Wang, H. Wang, F. Luo, S. Liao, *Electrochem. Energy Rev.* **2018**, *1*, 324–387.
- [5] S.-A. Chen, Y.-C. Liang, K.-T. Lu, C.-W. Pao, J.-F. Lee, T.-L. Lin, J.-M. Chen, *Phys. Chem. Chem. Phys.* **2014**, *16*, 3939–3945.
- [6] A. L. Danberry, B. Du, I.-S. Park, Y.-E. Sung, Y. Tong, *J. Am. Chem. Soc.* **2007**, *129*, 13806–13807.
- [7] a) H. W. Lei, S. Suh, B. Gurau, B. Workie, R. X. Liu, E. S. Smotkin, *Electrochim. Acta* **2002**, *47*, 2913–2919; b) C. Hartnig, E. Spohr, *Chem. Phys.* **2005**, *319*, 185–191; c) C. Hartnig, J. Grimminger, E. Spohr, *Electrochim. Acta* **2007**, *52*, 2236–2243.
- [8] a) M. Li, K. Duanmu, C. Wan, T. Cheng, L. Zhang, S. Dai, W. Chen, Z. Zhao, P. Li, H. Fei, Y. Zhu, R. Yu, J. Luo, K. Zang, Z. Lin, M. Ding, J. Huang, H. Sun, J. Guo, X. Pan, W. A. Goddard, P. Sautet, Y. Huang, X. Duan, *Nat. Catal.* **2019**, *2*, 495–503; b) S. Luo, L. Zhang, Y. Liao, L. Li, Q. Yang, X. Wu, X. Wu, D. He, C. He, W. Chen, Q. Wu, M. Li, E. J. M. Hensen, Z. Quan, *Adv. Mater.* **2021**, *33*, 2008508; c) Z. Zhang, J. Liu, J. Wang, Q. Wang, Y. Wang, K. Wang, Z. Wang, M. Gu, Z. Tang, J. Lim, T. Zhao, F. Ciucci, *Nat. Commun.* **2021**, *12*, 5235.
- [9] Y. Lu, J. Wang, L. Yu, L. Kovarik, X. Zhang, A. S. Hoffman, A. Gallo, S. R. Bare, D. Sokaras, T. Kroll, V. Dagle, H. Xin, A. M. Karim, *Nat. Catal.* **2019**, *2*, 149–156.
- [10] F. Li, L. Li, X. Liu, X. C. Zeng, Z. Chen, *ChemPhysChem* **2016**, *17*, 3170–3175.
- [11] a) J. Suntivich, Z. Xu, C. E. Carlton, J. Kim, B. Han, S. W. Lee, N. Bonnet, N. Marzari, L. F. Allard, H. A. Gasteiger, K. Hamad-Schifferli, Y. Shao-Horn, *J. Am. Chem. Soc.* **2013**, *135*, 7985–7991; b) W. Gong, Z. Jiang, R. Wu, Y. Liu, L. Huang, N. Hu, P. Tsiakaras, P. K. Shen, *Appl. Catal. B* **2019**, *246*, 277–283.
- [12] G. Vilé, D. Albani, M. Nachttegaal, Z. Chen, D. Dontsova, M. Antonietti, N. Lopez, J. Perez-Ramirez, *Angew. Chem. Int. Ed.* **2015**, *54*, 11265–11269; *Angew. Chem.* **2015**, *127*, 11417–11422.
- [13] a) J. Gu, M. Jian, L. Huang, Z. Sun, A. Li, Y. Pan, J. Yang, W. Wen, W. Zhou, Y. Lin, H.-J. Wang, X. Liu, L. Wang, X. Shi, X. Huang, L. Cao, S. Chen, X. Zheng, H. Pan, J. Zhu, S. Wei, W.-X. Li, J. Lu, *Nat. Nanotechnol.* **2021**, *16*, 1386–1393; b) X. Cui, H. Li, Y. Wang, Y. Hu, L. Hua, H. Li, X. Han, Q. Liu, F. Yang, L. He, X. Chen, Q. Li, J. Xiao, D. Deng, X. Bao, *Chem* **2018**, *4*, 1902–1910.
- [14] Z. Li, Y. Chen, S. Ji, Y. Tang, W. Chen, A. Li, J. Zhao, Y. Xiong, Y. Wu, Y. Gong, T. Yao, W. Liu, L. Zheng, J. Dong, Y. Wang, Z. Zhuang, W. Xing, C.-T. He, C. Peng, W.-C. Cheong,

- Q. Li, M. Zhang, Z. Chen, N. Fu, X. Gao, W. Zhu, J. Wan, J. Zhang, L. Gu, S. Wei, P. Hu, J. Luo, J. Li, C. Chen, Q. Peng, X. Duan, Y. Huang, X.-M. Chen, D. Wang, Y. Li, *Nat. Chem.* **2020**, *12*, 764–772.
- [15] X. Fang, Q. Shang, Y. Wang, L. Jiao, T. Yao, Y. Li, Q. Zhang, Y. Luo, H.-L. Jiang, *Adv. Mater.* **2018**, *30*, 1705112.
- [16] a) L. Zhang, Z.-J. Zhao, M. N. Banis, L. Li, Y. Zhao, Z. Song, Z. Wang, T.-K. Sham, R. Li, M. Zheng, J. Gong, X. Sun, *J. Mater. Chem. A* **2018**, *6*, 24397–24406; b) L. Zhang, R. Si, H. Liu, N. Chen, Q. Wang, K. Adair, Z. Wang, J. Chen, Z. Song, J. Li, M. N. Banis, R. Li, T.-K. Sham, M. Gu, L.-M. Liu, G. A. Botton, X. Sun, *Nat. Commun.* **2019**, *10*, 4936; c) N. Cheng, M. N. Banis, J. Liu, A. Riese, X. Li, R. Li, S. Ye, S. Knights, X. Sun, *Adv. Mater.* **2015**, *27*, 277–281.
- [17] a) J. Joo, T. Uchida, A. Cuesta, M. T. M. Koper, M. Osawa, *J. Am. Chem. Soc.* **2013**, *135*, 9991–9994; b) Y. X. Chen, A. Miki, S. Ye, H. Sakai, M. Osawa, *J. Am. Chem. Soc.* **2003**, *125*, 3680–3681; c) M. Heinen, Y.-X. Chen, Z. Jusys, R. J. Behm, *ChemPhysChem* **2007**, *8*, 2484–2489.
- [18] F. Kong, C. Du, J. Ye, G. Chen, L. Du, G. Yin, *ACS Catal.* **2017**, *7*, 7923–7929.
- [19] Y. Yao, S. Hu, W. Chen, Z.-Q. Huang, W. Wei, T. Yao, R. Liu, K. Zang, X. Wang, G. Wu, W. Yuan, T. Yuan, B. Zhu, W. Liu, Z. Li, D. He, Z. Xue, Y. Wang, X. Zheng, J. Dong, C.-R. Chang, Y. Chen, X. Hong, J. Luo, S. Wei, W.-X. Li, P. Strasser, Y. Wu, Y. Li, *Nat. Catal.* **2019**, *2*, 304–313.
- [20] R. Chattot, T. Asset, P. Bordet, J. Drnec, L. Dubau, F. Maillard, *ACS Catal.* **2017**, *7*, 398–408.
- [21] D. Kim, J. Resasco, Y. Yu, A. M. Asiri, P. Yang, *Nat. Commun.* **2014**, *5*, 4948.
- [22] a) Z. Yang, S. Pedireddy, H. K. Lee, Y. Liu, W. W. Tjiu, I. Y. Phang, X. Y. Ling, *Chem. Mater.* **2016**, *28*, 5080–5086; b) G.-R. Zhang, D. Zhao, Y.-Y. Feng, B. Zhang, D. S. Su, G. Liu, B.-Q. Xu, *ACS Nano* **2012**, *6*, 2226–2236.
- [23] a) N. Dimakis, N. E. Navarro, T. Mion, E. S. Smotkin, *J. Phys. Chem. C* **2014**, *118*, 11711–11722; b) L. Foppa, C. Coperet, A. Comas-Vives, *J. Am. Chem. Soc.* **2016**, *138*, 16655–16668; c) B. Hammer, Y. Morikawa, J. K. Norskov, *Phys. Rev. Lett.* **1996**, *76*, 2141–2144.
- [24] a) Q. Feng, S. Zhao, D. He, S. Tian, L. Gu, X. Wen, C. Chen, Q. Peng, D. Wang, Y. Li, *J. Am. Chem. Soc.* **2018**, *140*, 2773–2776; b) P. Ferrin, M. Mavrikakis, *J. Am. Chem. Soc.* **2009**, *131*, 14381–14389.

Manuscript received: May 23, 2022

Accepted manuscript online: August 29, 2022

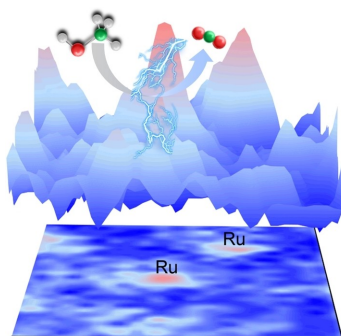
Version of record online: ■■, ■■

Research Articles

Single-Atom Catalysis

F. Kong, X. Liu, Y. Song, Z. Qian, J. Li,
L. Zhang, G. Yin, J. Wang,* D. Su,*
X. Sun* _____ e202207524

Selectively Coupling Ru Single Atoms to
PtNi Concavities for High-Performance
Methanol Oxidation via *d*-Band Center
Regulation



Single atom-cavity coupling enables the superior activity and stability of Ru single atoms tailored PtNi nano-catalysts towards methanol oxidation, synthesized by the selective ALD. The modulated *d*-band center and higher diffusion barrier accounts for the unparallel activity and stability on the Ru single atoms coupled to PtNi cavities, respectively.